Shape control of cathodized germanium oxide nanoparticles

Youcef A Bioud, Etienne Paradis, Abderraouf Boucherif, Dominique Drouin, Richard Arès

Shape control of cathodized germanium oxide nanoparticles

Youcef. A. Bioud[1,2*], Etienne Paradis[1], Abderraouf Boucherif[1], Dominique Drouin[1,2] and Richard Arès[1*]

[1] Laboratoire Nanotechnologies Nanosystèmes (LN2) – CNRS UMI-3463, Institut Interdisciplinaire d'Innovation Technologique (3IT), Université de Sherbrooke, 3000 Boulevard Université, Sherbrooke, J1K OA5 Québec, Canada

[2] Institut quantique, Département de physique, Université de Sherbrooke, Sherbrooke, J1K 2R1, Québec, Canada

Corresponding authors: y.bioud@usherbrooke.ca, richard.ares@usherbrooke.ca

Keywords: Electrodeposition, crystal growth, GeO_2 nanostructures, Cathodoluminescence.

Abstract

In this paper, hexagonal germanium dioxide (GeO_2) nanostructures with different morphologies and sizes were synthesized successfully by a simple and fast electrodeposition method. We investigated the electrochemical growth mechanism, the structural and optical properties of the products through Fourier transform infrared spectroscopy (FTIR), dispersive X-ray spectroscopy (EDX), X-ray diffraction (XRD) and cathodoluminescence (CL). The results reveal that the electrodeposited GeO_2 nanostructures are pure, dense, and highly crystalline. The XRD analyses indicate that grown GeO_2 crystals only shows peaks related to α-quartz structure. CL measurements exhibit strong blue and green lights emissions related to oxygen vacancies in the core of GeO_2 crystals. The obtained nanostructures may have potential application in future integrated optical devices.

Introduction

Nanoscale germanium-based materials exhibit a variety of novel properties and benefit a wide range of applications [1]–[10]. Germanium dioxide (GeO_2) nanostructures are versatile materials that have been explored in depth due to their unique thermal, optical and electrical properties. GeO_2 is thermally stable, has a high dielectric constant with large band gap energy (5 eV) [11], a high mechanical strength [12] and exhibits a refractive index that is slightly higher than that of SiO_2 [13], [14]. GeO_2 is also an attractive candidate for lithium-ion batteries (LIBs) due to its high theoretical reversible capacity (1125 mA h g^{-1} based on 4.25 mol Li per mol Ge) and low operating voltage, as well as long cyclability [15]–[17]. In addition, this nanomaterial shows a good blue photoluminescence behavior, which is highly sought after for optical waveguides and optoelectronic communication

devices [18], especially, electro optical modulators, piezoelectric glass materials, optical fibre materials and non-linear optics [19]–[21]. Due to this all, so far, different approaches to synthesizing nanostructured GeO_2 have been elucidated in the literature, including thermal treatment of Ge [22], vapor transport [23], carbothermal reaction [24], carbon nanotube confined reaction of Ge [25], chemical vapor deposition [26], supercritical fluid-liquid-solid synthesis [27], electro-spinning [28], e-beam evaporation [29], [30], sol-gel deposition [31], [32], radio frequency (RF) magnetron sputtering [33], [34], and laser ablation [35]. These techniques allow the synthesis of various GeO_2 shapes with tuned size such as nanoparticles, nanofibers, nanosheets [36], nanocubes, nanospindles, nanocapsules [37], [38], nanowires, nanorods [39], [40], and porous structures [41], [42]. However, GeO_2 nanoparticles fabricated from electrochemical processes have some distinctive advantages over nanoparticles fabricated by other methods mainly because (i) they are conveniently synthesized potentiostatic control, enabling electrophoretic deposition from the electrolyte, (ii) high density of nanocrystals, (iii) pure material (free of contaminants and chemical residues), (iv) high specific surface area, (v) coupled optical properties, (vi) can be transformed to powder by grinding and dispersed in a solution. In addition, the electrochemical process is standard, scalable that is already well integrated within an industrial fully automatic environment. Such a process meets the criteria, which provide an attractive solution for some specific applications.

This paper reports the successful synthesis of hexagonal GeO_2 nanostructures (nano-bundle aggregates and nanowires) by a simple and fast electrodeposition method with a plausible growth mechanism. The prepared GeO_2 nanostructures are characterized by scanning electron microscopy (SEM), Fourier transform infrared spectroscopy (FTIR), energy-

dispersive X-ray spectroscopy (EDX) and X-ray diffraction (XRD) measurements. Finally, we focus on performing a comprehensive optical characterization of GeO_2 nanostructures by cathodoluminescence (CL).

Experimental:

GeO_2 nanostructures synthesis was accomplished using a conventional three-electrode single-compartment electrochemical cell. GeO_2 nanostructures were potentiostatically deposited on p^+ type Ge wafers, (100) oriented with a nominal resistivity of 0.025 Ω cm (working electrode WE). A platinum sheet was used as counter-electrode (CE) and saturated calomel electrode (SCE) as reference electrode. All solutions were prepared from analytical grade reagents and double distilled water. As germanium tetrachloride ($GeCl_4$) is most widely used germanium source for germanium electrodeposition in ionic liquids, electrodeposition of GeO_2 was conducted in a hydrogen peroxide solution containing 10% of germanium tetrachloride solution ($GeCl_4$:H_2O_2, with the ratio of 1:9 by volume) at room temperature (20 °C). A wide range of GeO_2 morphology as a function of applied potentials was studied and a controlled structure, morphology and phase composition was sought. All potentials are reported with reference to the SCE scale. As surface conditions and activation are critical to electrocrystallisation nucleation and growth, Ge wafers were immersed in hydrofluoric acid (49%) to remove the native oxide before anodization. All deposition processes were carried out under stirring (700 rpm) using a cylindrical PTFE-coated magnetic stirrer bar of 12 mm long and 4.5 mm diameter with a pivot ring of 6 mm diameter, placed between the WE and the CE. At the end of the deposition process, all the wafers were rinsed with deionized water and dried under a high purity nitrogen gas flow. The chemical composition of the exposed surface is verified by energy-dispersive X-ray

(EDX) spectroscopy. Powder X-ray diffractograms have been measured with a Philips X'Pert diffractometer in the 2θ range from 10 to 65◦. The cathodoluminescence (CL) spectra and images are acquired at room temperature, in the same SEM setup as the one used for imaging the surface. Our CL system, in association with a spectrometer, allows monochromatic CL (GATAN MonoCL2) imaging as well as acquisition of CL spectra on localized spots of a sample with a spectral resolution of 0.5 nm. The accelerating voltage used in the CL characterization is 20 keV.

Results:

- *Electrochemical characterization and morphology:*

The electrochemical characterizations such as cyclic voltammetry measurements help us to identify oxidation reduction processes potentially undergone by the system of interest and to choose an appropriate potential [43], [44]. The electrochemical window of this ionic liquid was found to be 3.5 V (-2.0 V to 1.5 V) on platinum. Figure 1(a) shows cyclic voltammetry scan performed between -1.5 V to +0.5 V at a scan rate of 20 mV s^{-1}. The spectrum reveals a large reduction wave on the cathodic scan corresponds to two reduction reactions for Ge^{4+} ions: one leads to Ge^{2+} ions and the other to Ge [45]. The reduction waves at -0.6 and -1.1 V versus SCE were assigned to the reduction of Ge^{4+} to Ge^{2+} and Ge^{2+} to Ge, respectively [46]:

$$Ge^{4+} + 2e^{-} \rightarrow Ge^{2+} \qquad (1)$$

$$Ge^{2+} + 2e^{-} \rightarrow Ge \qquad (2)$$

The nucleation and growth of GeO_2 crystals are chemical steps and depend on the pH [47]. The nucleation started when the produced Ge^{2+} ions react with OH^- ions in the solution to form GeO_2:

$$Ge^{2+} + 2OH^- \rightarrow GeO_2 \downarrow + H_2 \qquad (3)$$

The current-time transients of the deposits produced at the -0.8, -1 and -1.2 V for the first 20 s were shown in figure 1(b). The shape of the curve can clearly indicate the nucleation-growth mechanism. At the beginning of the applied potentials, a high cathodic current was observed for a short time of 2 s compared to the deposition of 20 s which indicates the formation of GeO_2 on the surface of Ge substrate. The curves i(t) show also a normal dependence with the applied potential. The increase of the current density with the applied potential indicates that the process of the electrodeposition becomes faster. Figure 1(c-e) shows planar-view SEM images of the samples obtained at the -0.8, -1 and -1.2 V during 20s. The nanoparticles accumulate mostly on the side of the Ge wafer oriented toward the counter electrode during deposition. For all cathodic deposition potentials, the grains are assembled into a network of rounded agglomeration so-called “nano-bundle aggregates”. Their density increases by increasing the cathodic potential. A closer observation of an individual nano-bundle shows different forms and shapes: (i) a nanorod -like morphology at low deposition potential (-0.8 V), with a particle size of few nanometers (Fig. 1c), (ii) a mixt of nanowires and quartz-like at deposition potential of -1 V (Fig. 1d), and (iii) a pure quartz-like morphology at high deposition potential of -1.2 V (Fig. 1e). Similar GeO_2 shapes have been obtained by heating of Ge powders [48]. Figure 2(a) shows a defined edge of the formed GeO_2 with the rest of the substrate, indicating that the nanostructures are correctly and orderly electrodeposited on the emerged part of the substrate.

In order to understand the effect of current density on the growth mechanism, the deposition time is increased from 20 s to 300 s under the same applied potentials of -0.8 V, -1 V, and -1.2 V. The resulting forms are presented in Figs. 2b, 2c and 2d, respectively. The nanorods shape obtained at -0.8 V are transformed into a criss-cross network of nanowires with an average diameter of 200 nm and an average length of 3 microns. The mixed structure obtained at -1.0 V become denser with packed wire-like particles surrounding the spherical shapes. The dimensions of the nanowires are smaller than those at -0.8 V with a diameter ranging from 50 nm to 100 nm. The quartz-like shapes obtained at -1.2 V appears to be faceted or hexagonal submicrometer crystallites with typical diameters up to 1µm. The images show that the density and the dimension of the formed nanostructures increase with the deposition time, while the different morphology obtained at each applied potential reflects a growth mechanism differs. In fact, the growth often occurs according to the 1D growth mode at low potential (-0.8V) and to the 3D growth mode at high potential (-1.2V). However, the full process could be confirmed and better understood with further experimental work.

- *Chemical and structural Analyses*

In order to verify the chemical composition of the formed nanostructures, the samples were investigated and characterized through Fourier transform infrared spectroscopy (FTIR), energy-dispersive X-ray spectroscopy (EDX) and X-ray diffraction (XRD). Figure 3(a) shows the absorbance obtained by FTIR of bulk Ge sample after immersion in HF 49% solution. The dominant feature of this spectrum is at 2050 cm^{-1}, which corresponds to the stretching mode of the GeH_x bonds [49], [50]. GeH_x bending modes are also present and centered at 840 cm^{-1} [51]. Figure 3(b) shows the absorbance after anodization at -1.2 V during 300 s. The large band at 780 cm^{-1} is attributed to the vibration of Ge-O, assuming

an oxidized surface and/or GeO_2 precipitates [50], [51]. Vibrational measurements show clear evidence that following the anodization process; the hydrogen-terminated Ge surface is completely converted to contain GeO_x bonds.

Figures 4a-d and 4e-h show the EDX mapping of the electrodeposited samples at -0.8 V and -1.2 V, respectively. The figures reveal the uniform distribution of Ge and O contents in the formed nanowires and quartz structures. The enclosed EDX spectrum in Fig. 4i confirms the constituents of both nanostructures, which are only Ge and O since the characteristic peaks of Ge and O only appear in EDX spectra.

Powder XRD measurements were performed to investigate the crystal structure of the electrodeposited Ge oxide. The diffraction signals between 10° and 60° of the electrodeposited samples at -0.8 V and -1.2 V are shown in Fig. 5. All sharp peaks can be clearly determined as having a hexagonal GeO_2 with lattice constants of 4.98, 4.98, 5.64 (A°) and angles of (90°, 90°, 120°). No reflection peaks from impurities, such as unreacted Ge or other germanium oxides (tetragonal with a structure of rutile), were observed, within the detection limit of our technique (2-2.5 nm), indicating a high purity of the product [52]. The observed diffraction peaks from (100), (101), (110), and (102) planes can be indexed to those of the α-quartz GeO_2 (space group P3221) [53]. The intensity of the (101) peak is very strong and its width at half maximum is relatively narrow, indicating a good crystallization state.

- *Light emission from electrodeposited GeO_2 nanostructures*

To investigate the optical properties, GeO_2 nanostructures were examined by room-temperature cathodoluminescence spectroscopy. The morphology and CL characteristics

of the electrodeposited samples at -0.8 V and -1.2 V are reported on the spatial mapping (Fig. 6 a-d) which reveal luminescence only from the GeO_2 nanostructures. Fig. 6e shows the typical room temperature emission spectra from both samples. Two distinct emission peaks are observed in CL spectra, i.e. at 411 nm and 560 nm. The strong and dominated peak appeared at 560 nm (2.2 eV) can be related with the green emission while the presence of a broad peak at 411 nm (3.0 eV) can be referred as blue emission. Both blue and green light emissions are correlated to radiative recombination of defects in quartz-like GeO_2 crystals [18], [24], [54]. In fact, oxygen vacancies and germanium-related oxygen vacancies act as luminescence center and contribute to the observed luminescence from GeO_2 nanostructures such as single oxygen vacancy (OV) or double oxygen vacancy (DOV) [55]–[57]. No violet emission has been observed in the CL spectra from tetragonal GeO_2 crystals [48]. Because of their characteristic emission properties, these GeO_2 nanostructures may have potential application in future integrated optical devices.

Conclusions

In summary, tuning size and morphology of GeO_2 nanocrystals are made possible by electrodeposition. The formed nanostructures were characterized in detail in terms of their morphological, structural, and compositional properties which revealed that they are pure, grown in very high density, and highly crystalline. XRD analysis confirms the crystalline nature of the electrodeposited GeO_2 having α-quartz type hexagonal structure. The CL measurements showed that the structures have a strong blue and green light emissions assigned to radiative recombination of defects in GeO_2 crystals. This study demonstrates that the electrodeposition technique can be used for the synthesis of large quantity GeO_2

nanostructures which could be a promising candidate for the fabrication of cost-effective optoelectronics devices.

References:

[1] Wu, Songping, Cuiping Han, James Iocozzia, Mingjia Lu, Rongyun Ge, Rui Xu, and Zhiqun Lin. "Germanium-based nanomaterials for rechargeable batteries." Angewandte Chemie International Edition 55, no. 28 (2016): 7898-7922.

[2] Xia, Zhenyang, Haomin Song, Munho Kim, Ming Zhou, Tzu-Hsuan Chang, Dong Liu, Xin Yin et al. "Single-crystalline germanium nanomembrane photodetectors on foreign nanocavities." Science advances 3, no. 7 (2017): e1602783.

[3] Vaughn II, Dimitri D., and Raymond E. Schaak. "Synthesis, properties and applications of colloidal germanium and germanium-based nanomaterials." Chemical Society Reviews 42, no. 7 (2013): 2861-2879.

[4] Bioud, Youcef A., Meghan N. Beattie, Abderraouf Boucherif, Mourad Jellit, Romain Stricher, Serge Ecoffey, Gilles Patriarche et al. "A porous Ge/Si interface layer for defect-free III-V multi-junction solar cells on silicon." In Physics, Simulation, and Photonic Engineering of Photovoltaic Devices VIII, vol. 10913, p. 109130T. International Society for Optics and Photonics, 2019. doi: 10.1117/12.2511080

[5] Bioud, Youcef A., Abderraouf Boucherif, Etienne Paradis, Ali Soltani, Dominique Drouin, and Richard Arès. "Low cost Ge/Si virtual substrate through dislocation trapping by nanovoids." arXiv preprint arXiv:1805.05621 (2018). arXiv:1805.05621

[6] Bioud, Youcef A., Abderraouf Boucherif, Ali Belarouci, Etienne Paradis, Simon Fafard, Vincent Aimez, Dominique Drouin, and Richard Arès. "Fast growth synthesis of mesoporous germanium films by high frequency bipolar electrochemical etching." Electrochimica Acta 232 (2017): 422-430.

[7] Beattie, Meghan N., Youcef A. Bioud, David G. Hobson, Abderraouf Boucherif, Christopher E. Valdivia, Dominique Drouin, Richard Arès, and Karin Hinzer. "Tunable conductivity in mesoporous germanium." Nanotechnology 29, no. 21 (2018): 215701.

[8] Bioud, Youcef A., Maxime Rondeau, Abderraouf Boucherif, Gilles Patriarche, Dominique Drouin, and Richard Arès. "Effect of sintering germanium epilayers on dislocation dynamics: From theory to experimental observation." Acta Materialia 200 (2020): 608-618.

[9] Bioud, Youcef A., Abderraouf Boucherif, Maksym Myronov, Ali Soltani, Gilles Patriarche, Nadi Braidy, Mourad Jellite, Dominique Drouin, and Richard Arès. "Uprooting defects to enable high-performance III–V optoelectronic devices on silicon." Nature communications 10, no. 1 (2019): 1-12.

[10] Bioud, Youcef A., Abderraouf Boucherif, Gilles Patriarche, Dominique Drouin, and Richard Arès. "Engineering dislocations and nanovoids for high-efficiency III–V photovoltaic cells on silicon." In AIP Conference Proceedings, vol. 2298, no. 1, p. 020002. AIP Publishing LLC, 2020. https://doi.org/10.1063/5.0033162

[11] Zhang, Siwen, Bosi Yin, Yang Jiao, Yang Liu, Xu Zhang, Fengyu Qu, Ahmad Umar, and Xiang Wu. "Ultra-long germanium oxide nanowires: Structures and optical properties." Journal of alloys and compounds 606 (2014): 149-153.

[12] Ramana, C. V., G. Carbajal-Franco, R. S. Vemuri, I. B. Troitskaia, S. A. Gromilov, and V. V. Atuchin. "Optical properties and thermal stability of germanium oxide (GeO_2) nanocrystals with α-quartz structure." Materials Science and Engineering: B 174, no. 1-3 (2010): 279-284.

[13] Chiasera, A., C. Macchi, S. Mariazzi, S. Valligatla, Lorenzo Lunelli, Cecilia Pederzolli, D. N. Rao, A. Somoza, R. S. Brusa, and M. Ferrari. "CO_2 Laser irradiation of GeO_2 planar waveguide fabricated by rf-sputtering." Optical Materials Express 3, no. 9 (2013): 1561-1570. https://doi.org/10.1364/OME.3.001561

[14] Hsu, Cheng-Hsing, Jenn-Sen Lin, Yi-Da He, Shu-Fong Yang, Pai-Chuan Yang, and Wen-Shiush Chen. "Optical, electrical properties and reproducible resistance switching of GeO2 thin films by sol–gel process." Thin Solid Films 519, no. 15 (2011): 5033-5037.

[15] Ngo, Duc Tung, Ramchandra S. Kalubarme, Hang TT Le, Choong-Nyeon Park, and Chan-Jin Park. "Conducting additive-free amorphous GeO_2/C composite as a high capacity and long-term stability anode for lithium ion batteries." Nanoscale 7, no. 6 (2015): 2552-2560.

[16] Qiu, Heyuan, Lingxing Zeng, Tongbin Lan, Xiaokun Ding, and Mingdeng Wei. "In situ synthesis of GeO 2/reduced graphene oxide composite on Ni foam substrate as a binder-free anode for high-capacity lithium-ion batteries." Journal of Materials Chemistry A 3, no. 4 (2015): 1619-1623.

[17] Hwang, Jongkook, Changshin Jo, Min Gyu Kim, Jinyoung Chun, Eunho Lim, Seongseop Kim, Sanha Jeong, Youngsik Kim, and Jinwoo Lee. "Mesoporous Ge/GeO_2/carbon lithium-ion battery anodes with high capacity and high reversibility." ACS nano 9, no. 5 (2015): 5299-5309.

[18] Armelao, Lidia, Franziskus Heigl, Pil-Sook Grace Kim, Richard A. Rosenberg, Tom Z. Regier, and Tsun-Kong Sham. "Visible emission from GeO_2 nanowires: site-specific insights via X-ray excited optical luminescence."

The Journal of Physical Chemistry C 116, no. 26 (2012): 14163-14169.
[19] Lignie, Adrien, Pascale Armand, and Philippe Papet. "Growth of piezoelectric water-free GeO_2 and SiO_2-substituted GeO2 single-crystals." Inorganic chemistry 50, no. 19 (2011): 9311-9317.
[20] Chang, T. C., S. T. Yan, C. H. Hsu, M. T. Tang, J. F. Lee, Ya-Hsiang Tai, Po-Tsun Liu, and S. M. Sze. "A distributed charge storage with GeO_2 nanodots." Applied physics letters 84, no. 14 (2004): 2581-2583.
[21] Hermet, Patrick, Guillaume Fraysse, Adrien Lignie, Pascale Armand, and Ph Papet. "Density functional theory predictions of the nonlinear optical properties in α-Quartz-type germanium dioxide." The Journal of Physical Chemistry C 116, no. 15 (2012): 8692-8698.
[22] Kim, Hyoun Woo, Jong Woo Lee, Mesfin Abayneh Kebede, Hyo Sung Kim, and Chongmu Lee. "Catalyst-free synthesis of GeO_2 nanowires using the thermal heating of Ge powders." Current Applied Physics 9, no. 6 (2009): 1300-1303.
[23] Wu, Yiying, and Peidong Yang. "Germanium nanowire growth via simple vapor transport." Chemistry of Materials 12, no. 3 (2000): 605-607.
[24] Wu, X. C., W. H. Song, B. Zhao, Y. P. Sun, and J. J. Du. "Preparation and photoluminescence properties of crystalline GeO_2 nanowires." Chemical Physics Letters 349, no. 3-4 (2001): 210-214.
[25] Zhang, Yingjiu, Jing Zhu, Qi Zhang, Yunjie Yan, Nanlin Wang, and Xiaozhong Zhang. "Synthesis of GeO2 nanorods by carbon nanotubes template." Chemical Physics Letters 317, no. 3-5 (2000): 504-509.
[26] Mathur, Sanjay, Hao Shen, Vladimir Sivakov, and Ulf Werner. "Germanium nanowires and core− shell nanostructures by chemical vapor deposition of [Ge (C5H5) 2]." Chemistry of materials 16, no. 12 (2004): 2449-2456.
[27] Hanrath, Tobias, and Brian A. Korgel. "Supercritical fluid–liquid–solid (SFLS) synthesis of Si and Ge nanowires seeded by colloidal metal nanocrystals." Advanced Materials 15, no. 5 (2003): 437-440.
[28] Kim, H. Y., P. Viswanathamurthi, Narayan Bhattarai, and D. R. Lee. "Preparation and morphology of germanium oxide nanofibers." Reviews on Advanced Materials Science 5, no. 3 (2003): 220-223.
[29] Saikiran, V., N. Srinivasa Rao, G. Devaraju, G. S. Chang, and A. P. Pathak. "Formation of Ge nanocrystals from ion-irradiated GeO_2 nanocrystals by swift Ni ion beam." Nuclear Instruments and Methods in Physics Research Section B: Beam Interactions with Materials and Atoms 312 (2013): 1-6.
[30] Krupanidhi, S. B., M. Sayer, and A. Mansingh. "Electrical characterization of amorphous germanium dioxide films." Thin solid films 113, no. 3 (1984): 173-184.
[31] Zhang, Xuehua, Wenxiu Que, Jing Chen, Jiaxing Hu, and Weiguo Liu. "Concave micro-lens arrays fabricated from the photo-patternable GeO_2/ormosils hybrid sol–gel films." Optical Materials 35, no. 12 (2013): 2556-2560.
[32] Zhang, Lin, Geng Chen, Bowei Chen, Tianshi Liu, Yang Mei, and Xuan Luo. "Monolithic germanium oxide aerogel with the building block of nano-crystals." Materials Letters 104 (2013): 41-43.
[33] Terakado, Nobuaki, and Keiji Tanaka. "Photo-induced phenomena in sputtered GeO2 films." Journal of non-crystalline solids 351, no. 1 (2005): 54-60.
[34] Rana, Mukti M., and Donald P. Butler. "Noise reduction of a-Si1− xGexOy microbolometers by forming gas passivation." Thin Solid Films 516, no. 18 (2008): 6499-6503.
[35] Lauhon, Lincoln J., Mark S. Gudiksen, Deli Wang, and Charles M. Lieber. "Epitaxial core–shell and core–multishell nanowire heterostructures." Nature 420, no. 6911 (2002): 57-61.
[36] Nejaty-Moghadam, Laya, Azade Esmaeili-Bafghi-Karimabad, Sousan Gholamrezaei, Masood Hamadanian, and Masoud Salavati-Niasari. "Facile synthesis of GeO_2 nanostructures and measurement of photocatalytic, photovoltaic and photoluminescence properties." Journal of Materials Science: Materials in Electronics 26, no. 9 (2015): 6386-6394.
[37] Wu, H. P., J. F. Liu, M. Y. Ge, L. Niu, Y. W. Zeng, Y. W. Wang, G. L. Lv, L. N. Wang, G. Q. Zhang, and J. Z. Jiang. "Preparation of monodisperse GeO_2 nanocubes in a reverse micelle system." Chemistry of Materials 18, no. 7 (2006): 1817-1820.
[38] Adachi, Motonari, Keizo Nakagawa, Kensuke Sago, Yusuke Murata, and Yukihiro Nishikawa. "Formation of GeO_2 nanosheets using water thin layers in lamellar phase as a confined reaction field—in situ measurement of SAXS by synchrotron radiation." Chemical communications 18 (2005): 2381-2383. https://doi.org/10.1039/B419017C
[39] Hidalgo, P., B. Méndez, and J. Piqueras. "High aspect ratio GeO2 nano-and microwires with waveguiding behaviour." Nanotechnology 18, no. 15 (2007): 155203. https://doi.org/10.1088/0957-4484/18/15/155203
[40] Kim, Won Jeon, Veronika Soshnikova, Josua Markus, Keun Hyun Oh, Gokulanathan Anandapadmanaban, Ramya Mathiyalagan, Zuly Elizabeth Jimenez Perez, Yeon Ju Kim, and Deok Chun Yang. "Room temperature synthesis of germanium dioxide nanorods and their in vitro photocatalytic application." Optik 178 (2019): 664-668.
[41] Wei, Wei, Fangfang Jia, Peng Qu, Zhongning Huang, Hua Wang, and Lin Guo. "Morphology memory but reconstructing crystal structure: porous hexagonal GeO_2 nanorods for rechargeable lithium-ion batteries." Nanoscale 9, no. 11 (2017): 3961-3968.
[42] Zou, Xiaodong, Tony Conradsson, Miia Klingstedt, Mike S. Dadachov, and Michael O'Keeffe. "A mesoporous germanium oxide with crystalline pore walls and its chiral derivative." Nature 437, no. 7059 (2005): 716-719.

[43] Mahenderkar, Naveen K., Ying-Chau Liu, Jakub A. Koza, and Jay A. Switzer. "Electrodeposited germanium nanowires." ACS nano 8, no. 9 (2014): 9524-9530.

[44] Laidoudi, S., A. Y. Bioud, A. Azizi, G. Schmerber, J. Bartringer, S. Barre, and A. Dinia. "Growth and characterization of electrodeposited Cu2O thin films." Semiconductor science and technology 28, no. 11 (2013): 115005. https://doi.org/10.1088/0268-1242/28/11/115005

[45] Wu, Minxian, Neil R. Brooks, Stijn Schaltin, Koen Binnemans, and Jan Fransaer. "Electrodeposition of germanium from the ionic liquid 1-butyl-1-methylpyrrolidinium dicyanamide." Physical Chemistry Chemical Physics 15, no. 14 (2013): 4955-4964.

[46] Meng, Xiangdong, Rihab Al-Salman, Jiupeng Zhao, Natalia Borissenko, Yao Li, and Frank Endres. "Electrodeposition of 3D ordered macroporous germanium from ionic liquids: a feasible method to make photonic crystals with a high dielectric constant." Angewandte Chemie International Edition 48, no. 15 (2009): 2703-2707.

[47] Pourbaix, Marcel. "Atlas of electrochemical equilibria in aqueous solution." NACE 307 (1974).

[48] Kim, Hyoun Woo, and Jong Woo Lee. "GeO_2 nanostructures fabricated by heating of Ge powders: Pt-catalyzed growth, structure, and photoluminescence." Physica E: Low-dimensional Systems and Nanostructures 40, no. 7 (2008): 2499-2503.

[49] Park, Kibyung, Younghwan Lee, and Sangwoo Lim. "Modification of H-terminated Ge surface in hydrochloric acid." Applied Surface Science 254, no. 6 (2008): 1842-1846.

[50] De Gryse, Olivier, Jan Vanhellemont, and Paul Clauws. "Determination of oxide precipitate phase and morphology in silicon and germanium using infra-red absorption spectroscopy." Materials science in semiconductor processing 9, no. 1-3 (2006): 246-251.

[51] Rivillon, Sandrine, Yves J. Chabal, Fabrice Amy, and Antoine Kahn. "Hydrogen passivation of germanium (100) surface using wet chemical preparation." Applied Physics Letters 87, no. 25 (2005): 253101.

[52] Jing, Chengbin, Jinxia Hou, and Yongheng Zhang. "Morphology controls of GeO_2 particles precipitated by a facile acid-induced decomposition of germanate ions in aqueous medium." Journal of crystal growth 310, no. 2 (2008): 391-396.

[53] Jing, Chengbin, Wei Sun, Wei Wang, Yi Li, and Junhao Chu. "Morphology and crystal phase evolution of GeO2 in liquid phase deposition process." Journal of crystal growth 338, no. 1 (2012): 195-200.

[54] Jawad, M. J., M. R. Hashim, and N. K. Ali. "Synthesis, structural, and optical properties of electrochemically deposited GeO2 on porous silicon." Electrochemical and Solid State Letters 14, no. 2 (2010): D17. https://doi.org/10.1149/1.3516605

[55] Zacharias, M., and P. M. Fauchet. "Blue luminescence in films containing Ge and GeO_2 nanocrystals: the role of defects." Applied Physics Letters 71, no. 3 (1997): 380-382.

[56] Seal, M., N. Bose, and S. Mukherjee. "Application of GeO_2 nanoparticle as electrically erasable memory and its photo catalytic behaviour." Materials Research Express 5, no. 6 (2018): 065007. https://doi.org/10.1088/2053-1591/aac66b

[57] Jiang, Z., T. Xie, G. Z. Wang, X. Y. Yuan, C. H. Ye, W. P. Cai, G. W. Meng, G. H. Li, and L. D. Zhang. "GeO_2 nanotubes and nanorods synthesized by vapor phase reactions." Materials Letters 59, no. 4 (2005): 416-419.

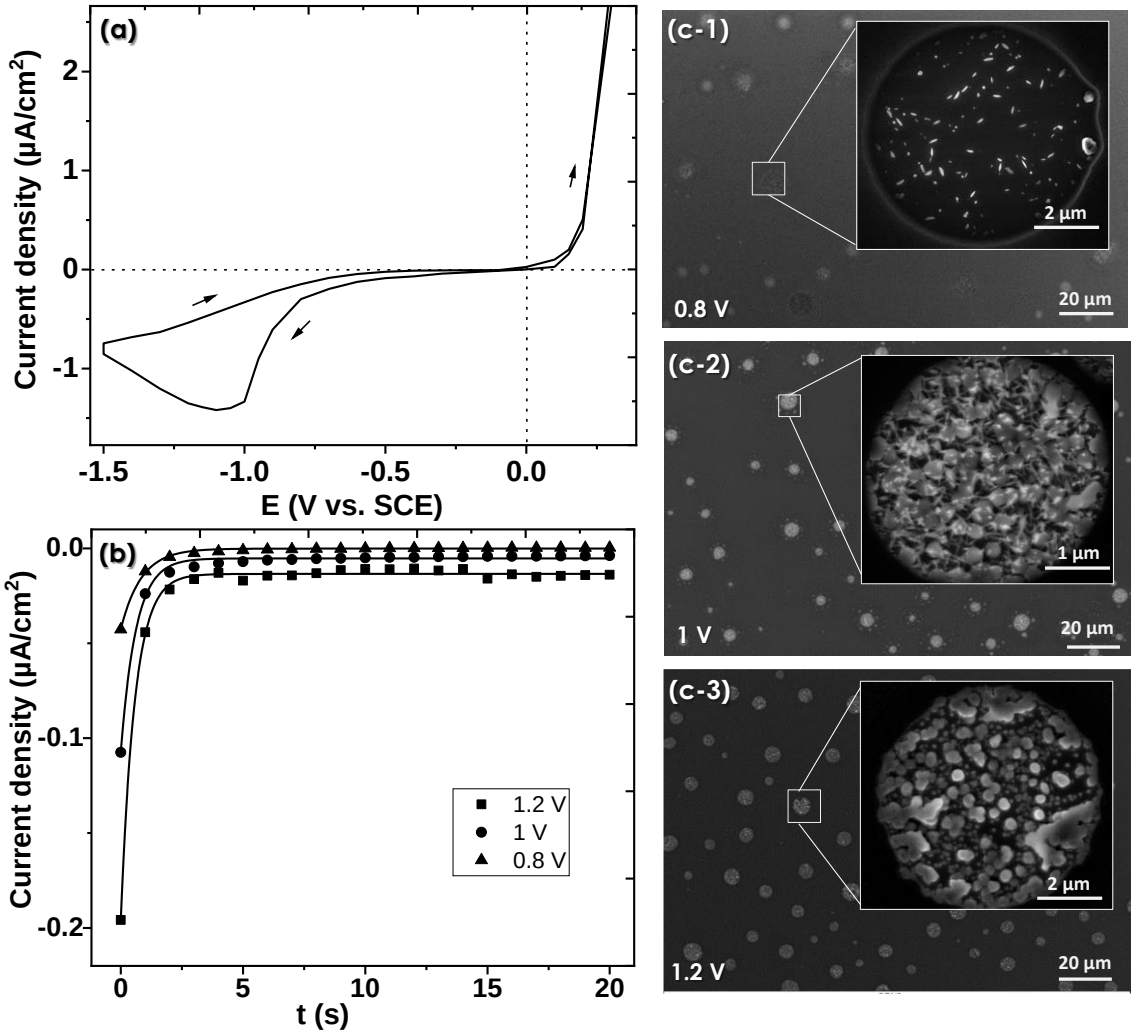

Fig. 1: (a) Cyclic voltammogram recorded in a $GeCl_4$:H_2O_2 solution, with the ratio of 1:9 by volume. The potential scan rate is 20 mV s^{-1}. (b) Current transients for GeO_2 nanostructures deposited at different applied potentials. Planar-view SEM images of GeO_2 nano-structures electrodeposited at -0.8 V (c), -1 V (d) and -1.2 V (e) on Ge substrate during 20 s.

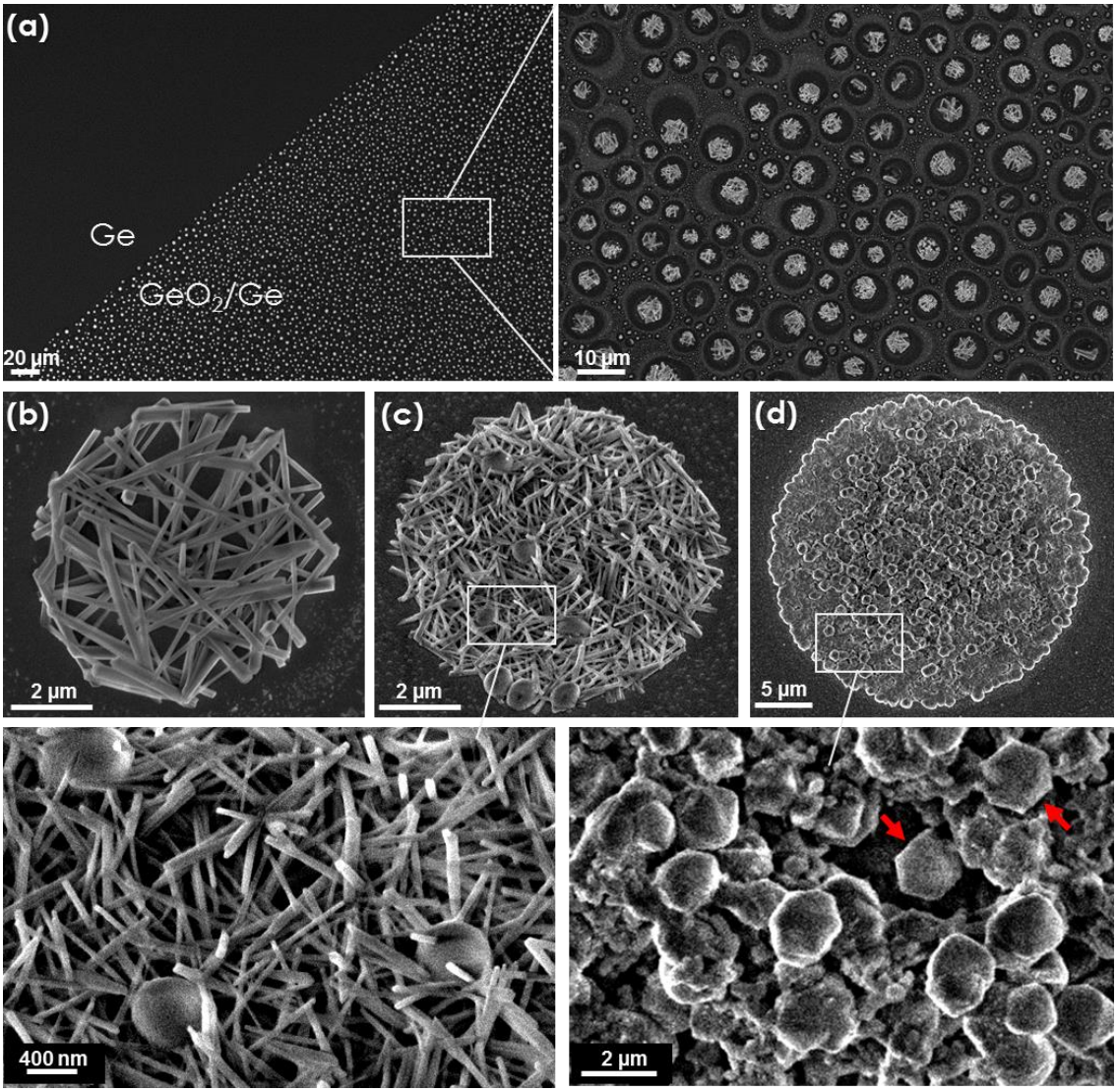

Fig. 2: Planar-view SEM images shown the emerged substrate limit in the electrolyte (a) of GeO_2 nano-structures electrodeposited at -0.8 V (b), -1 V (c) and -1.2 V (d) on Ge substrate during 300 s. The inset shows high-resolution SEM image on the nano-assembled structures.

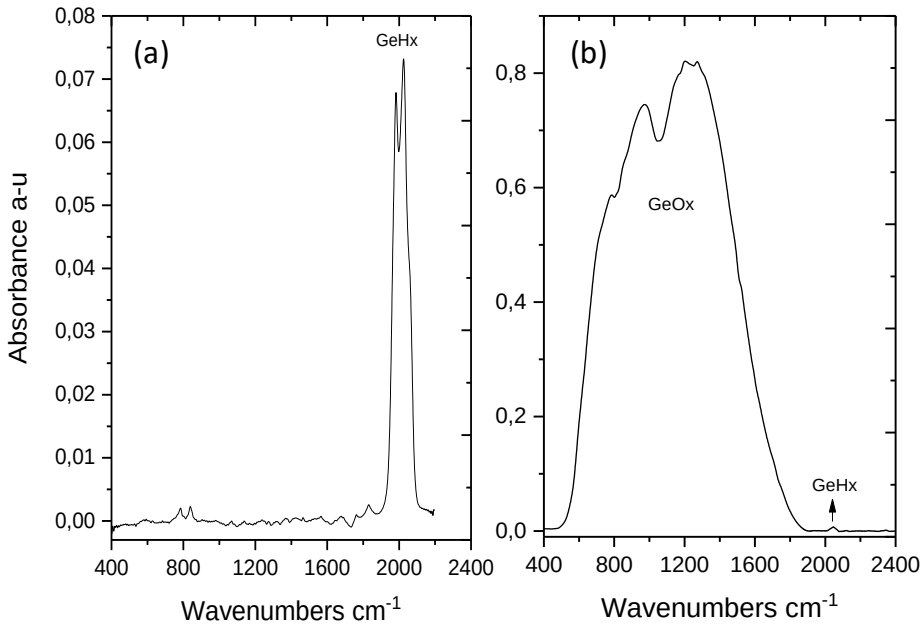

Figure 3: Typical transmission-FTIR spectra of the Ge surface before (a) and after electrodeposition of GeO_2 nanostructures at -1.2 V during 300 s (b), which is dominated by a large band correlated to the vibration of Ge-O bonds.

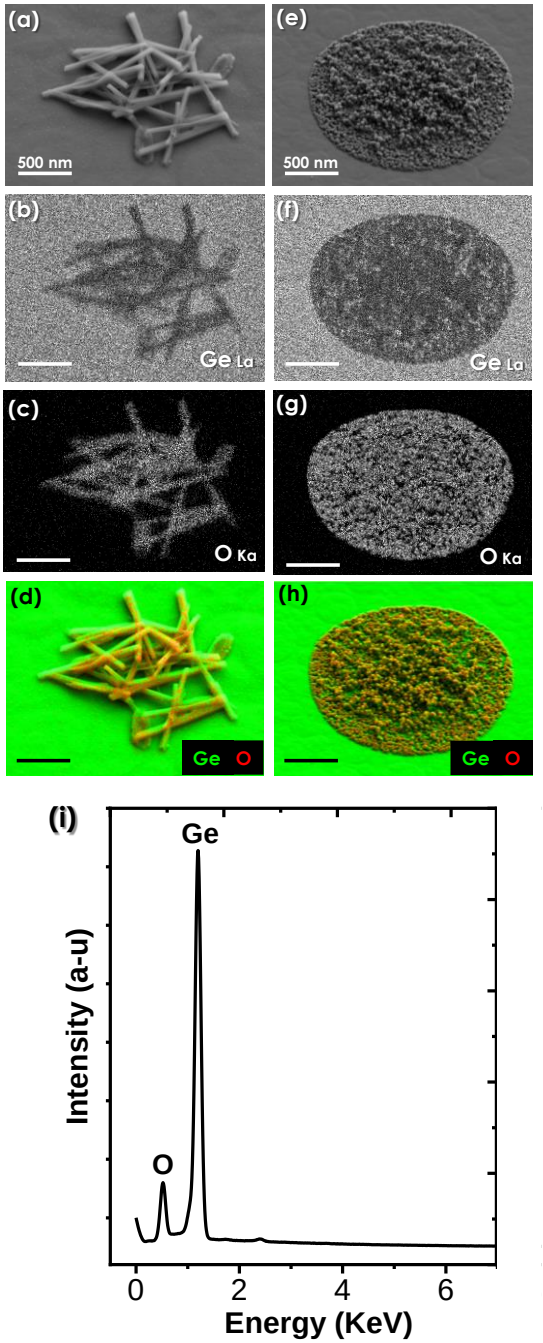

Fig. 4: EDX mapping of GeO_2 nanowires (a) and quartz structures (e) electrodeposited at 0.8 V and 1.2 V respectively. The top view SEM image and the EDX element maps for (b,c) Ge, (f,g) O elements, (d,h) a mixture of Ge and O and (i) EDX spectra acquired in SEM at the top view sample.

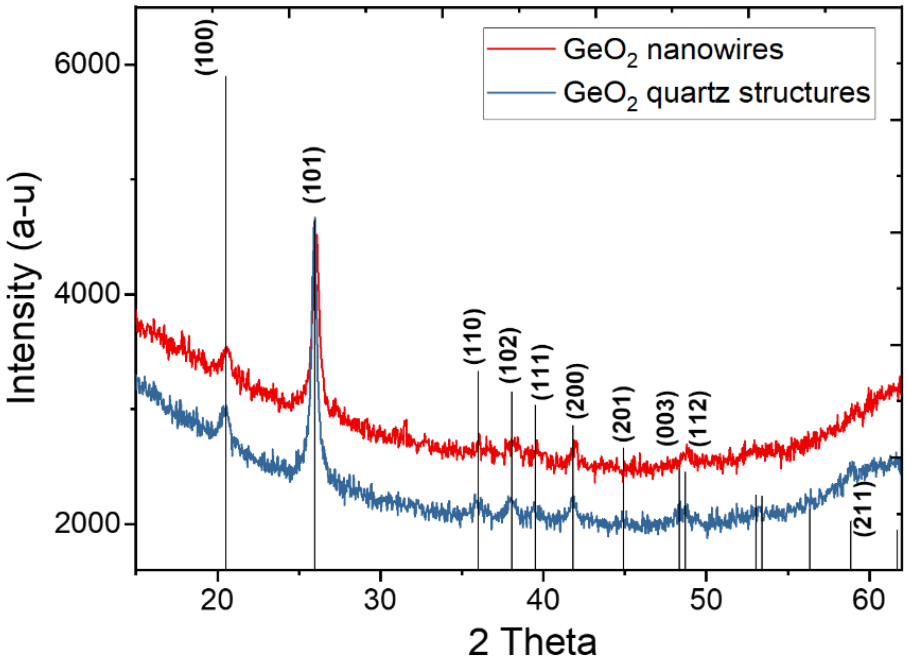

Fig. 5: Powder XRD of GeO_2 nanowires and quartz structures electrodeposited at 0.8 V and 1.2 V respectively.

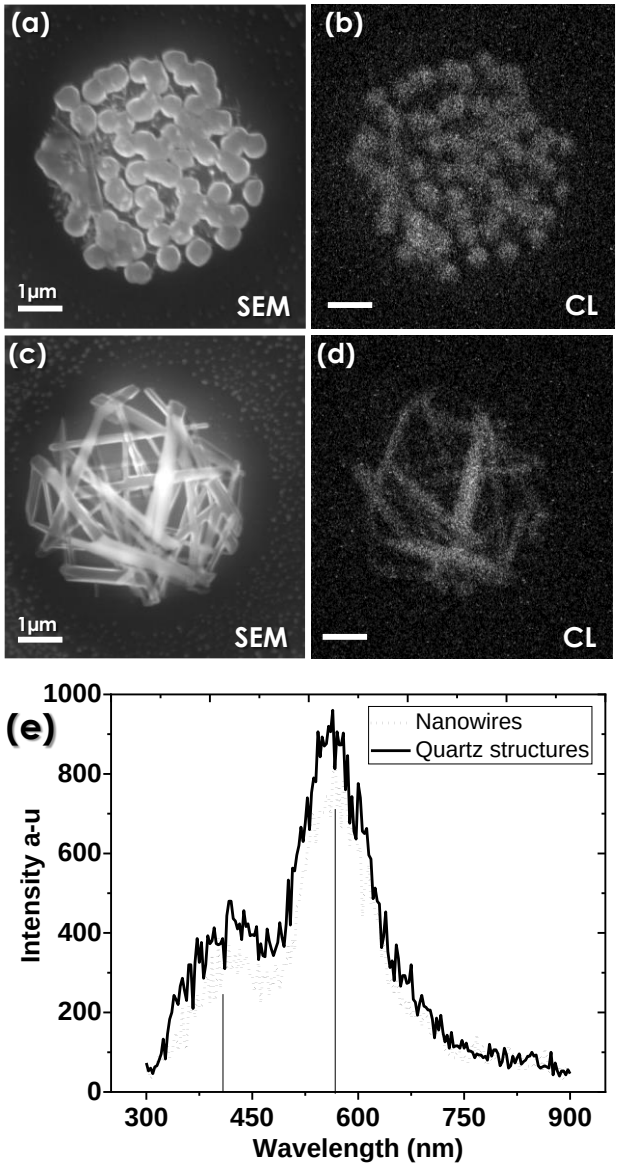

Fig. 6: SEM and CL micrographs taken from the top surface of GeO_2 nanowires (a,b) and quartz structures (c, d) electrodeposited at 0.8 V and 1.2 V respectively. (e) The corresponding CL spectra.